Conductor Temperature Estimation and Prediction at Thermal Transient State in Dynamic Line Rating Application

David L. Alvarez, *Student Member, IEEE,* F. Faria da Silva *Member, IEEE,* Enrique E. Mombello *Senior Member, IEEE,* Claus Leth Bak *Senior Member, IEEE,* and Javier A. Rosero *Member, IEEE,*

***Abstract*—The traditional methodology for defining the ampacity of overhead lines is based on conservative criteria regarding the operating conditions of the line, leading to the so-called static line rating. Although this procedure has been considered satisfactory for decades, it is nowadays sensible to account for more realistic line operating conditions when calculating its dynamic ampacity. Dynamic line rating is a technology used to improve the ampacity of overhead transmission lines based on the assumption that ampacity is not a static value but a function of weather and line's operating conditions. In order to apply this technology, it is necessary to monitor and predict the temperature of the conductor over time by direct or indirect measurements. This paper presents an algorithm to estimate and predict the temperature in overhead line conductors using an Extended Kalman Filter, with the aim of minimizing the mean square error in the current and subsequent states (temperature) of the conductor. The proposed algorithm assumes both actual weather and current intensity flowing along the conductor as control variables. The temperature of the conductor, mechanical tension and sag of the catenary are used as measurements because the common practice is to measure these values with dynamic line rating hardware. The algorithm has been validated by both simulations and measurements. The results of this study conclude that it is possible to implement the algorithm into Dynamic Line Rating systems, leading to a more accurate estimation and prediction of temperature.**

***Index Terms*—Dynamic Line Rating (DLR), Dynamic State Estimation, Extended Kalman Filter (EKF), Overhead Line (OHL)**

I. Introduction

WITH the constant increase in power consumption, an upgrade and update of current assets are necessary for control and operation of existing power networks. As a result of the advances in renewable power generation, such as wind and solar energy, there exists a constant growth in new power plants. Therefore, bottlenecks are arising in transmission level, mainly in overhead lines (OHLs), which are facing economic, social, political and implementation time challenges. In order to reduce both congestion and face these challenges, different techniques [1] can be used depending on the characteristics of the line. Among these solutions is monitoring the line state allowing the assessment of thermal limits and the application of DRL [2], as long as the ampacity is limited by the sag of the catenary. As the forerunner of DLR, OHL's ampacity by probabilistic methods was introduced using seasonal atmospheric conditions [3]. Subsequently, the monitoring of OHL's thermal state was reached using information technologies.

Because of only one span in an OHL can limit the ampacity and its behavior depends on the adjacent suspension spans, this set of spans is assumed monitored for DLR. This set is commonly known as the critical stringing section. However, this section can change over time as a result of weather variations. Consequently, different methodologies can be used to identify critical stringing sections and to define DLR devices location [4], [5].

In OHLs, two types of thermal limits are defined. The first one is related to thermal equilibrium (steady state) and used for planning and control. The second one is related to transient state and given by a relationship between current intensity and time; this limit is used for contingencies assessment during operation. Using DLR, the data required to define these two limits are historic reports of weather or low scale atmospheric models based on local measurements [6] and direct measurements in critical stringing sections whether of sag length, mechanical tension, inclination, clearance, among others [7].

The ampacity limit at steady state using DLR can estimate with weather forecast [8]. On the other hand, to compute dynamic limits (at thermal transient state) with DLR, it is necessary to know on-line both the conductor temperature and the atmospheric conditions. To this end, some techniques are proposed, such as computing wind speed from direct measurements [9] or including a weather station together with the direct monitoring device [10]. However, given the nature of the atmospheric conditions, which vary in space and time and the uncertainty in the parameters of the OHL, an inaccuracy is obtained in the ampacity when the temperature is used [11].

The variation in the atmospheric conditions along a stringing section can be modeled by the average conductor temperature with an effective wind speed in order to avoid spot temperature [12]. The impact of data uncertainty is addressed in the literature. For instance, the uncertainties in input data as well as in the parameters used in heat transfer models are addressed by affine arithmetic in [13]. Similarly, robust

David L. Alvarez and Javier A. Rosero are with the Departamento de Ingeniería Eléctrica y Electrónica, Facultad de Ingeniería, Universidad Nacional de Colombia, Bogotá, Colombia (dlalvareza@unal.edu.co - jaroserog@unal.edu.co)

F. Faria da Silva and Claus Leth Bak are with the Department of Energy Technology, Aalborg University, Aalborg, Denmark (ffs@et.aau.dk - clb@et.aau.dk

Enrique E. Mombello is with the Instituto de Energía Eléctrica, CONICET, Universidad Nacional de San Juan, San Juan, Argentina (mombello@iee.unsj.edu.ar)

corrective control measures considering the weather forecast uncertainty is used in reference [14]. The impact of the uncertainty in both the catenary parameters and temperature in the calculation of the sag is analyzed in [15]. An enhanced methodology is presented in [16] using on-line information of a self-organized sensor network. This network uses temperature sensors and has the ability to predict, estimate and validate information used for DLR. In this way, this paper presents a state estimation algorithm for DLR at thermal transient state which allows to estimate and predict the average conductor temperature of stringing sections. The algorithm is based on an Extended Kalman Filter (EKF), and it has the advantage of using available DLR systems. To implement the EKF, it is provided that the set of critical stringing sections are monitored by DLR hardware and their atmospheric conditions are known.

The motivation to propose this algorithm is that currently used methods to minimize errors in the estimation of temperature in OHLs [17], [18], [19] are probably not the best choice for on-line dynamic state estimation during thermal transients. With the EKF, estimation and prediction of both states and parameters of nonlinear dynamic systems is reached [20]. Additionally, the uncertainties in the atmospheric conditions, the current intensity and the direct measurements are considered by the proposed EKF with the computing of covariance propagation matrix and the Kalman gain. The state variables of the proposed EKF are the average conductor temperature, the average effective wind speed, the emissivity and the solar absorptivity of conductor surface. The average temperature was chosen because it is possible to estimate the OHL ampacity with this value. The consideration of additional parameters leads to improvements in temperature prediction, since wind speed has the greatest impact on cooling [12], and emissivity and absorptivity commonly present a high uncertainty [21].

This paper is organized as follows: Section II provides a brief introduction to heat transfer in OHL's conductor and to direct measurements used in DLR. Section III introduces the algorithm developed. Section IV presents a case study and experimental test carried out with the aim of evaluating the performance of the algorithm. Finally, conclusions are presented in section V.

II. Background

Thermal behavior of OHLs is determined by heat transfer as a result of heat gains and heat losses. This phenomenon affects the thermal, electrical, and mechanical characteristics of OHLs. Consequently, it is possible to estimate the thermal state of the conductor by monitoring these physical changes.

A. Heat Transfer at Transient State

Heat transfer in OHL conductors is a well-known process [22] and is described in standards and guides [21], [23]. The main equation for this process is

$$\frac{dT_S}{dt} = \frac{{i_{km}}^2 R\left(T_S\right) + q_s - q_c\left(T_S\right) - q_r\left(T_S\right)}{mC_p} \tag{1}$$

where T_S is the temperature of the conductor at the surface, i_{km} is the current intensity, R is the ac electrical resistance per unit length, q_s is the solar heating, q_c is the convective cooling, q_r is the radiative cooling, m is the mass per unit length and C_p is the specific heat capacity of the conductor. Equation (1) can solve by numerical integration by using

$$\Delta T_S = \frac{{i_{km}}^2 R\left(T_S\right) + q_s - q_c\left(T_S\right) - q_r\left(T_S\right)}{mC_p}\Delta t \tag{2}$$

taking time intervals Δt, provided that the initial temperature, the thermal parameters of the conductor and the atmospheric conditions along the integration time are known. The computing time to calculate temperature by this numerical method is not a problem with modern computers, because under contingencies or normal operation the thermal constant of the conductors is higher (commonly 15 min) than the processing time used to solve it (less than 1 s).

The maximum current intensity ($|i_{km}|_{max}$) at conductor reach the thermal equilibrium can compute using the maximum allowable conductor temperature ($T_{S_{max}}$) as follow

$$|i_{km}|_{max} = \sqrt{\frac{q_c\left(T_{S_{max}}\right) + q_r\left(T_{S_{max}}\right) - q_s}{R\left(T_{S_{max}}\right)}} \tag{3}$$

Thus, OHL's ampacity can be estimated using both static or dynamic line ratings. For contingencies management, commonly the maximum current intensity vs time plot is computed solving (1) until the conductor reach the maximum allowable temperature for different values of i_{km}.

B. Direct Measurements for DLR

Although (1) correctly models the behavior of temperature in OHL's conductors, there exist uncertainties in the computing results because of inaccuracies in the inputs and parameters. Thus, direct measurements for DLR are required in critical stringing sections to enhance the accuracy. With these measurements, the thermal state is measured discretely by taking samples between 1 min and 10 min [12], allowing a thermal monitoring. Direct measurements are classified by CIGRE [7] into temperature, sag and mechanical tension. From measurements of these variables, the temperature of the conductor is computed using known relationships, such as the state equation (temperature related to tension) and the catenary equation (related tension with sag). Although the conductor temperature can be directly monitored, the monitoring system has errors produced whether by changes in the temperature along the span, the influence of measurement devices over the spot where the reading is taken, uncertainties in the catenary parameters such as the mechanical tension reference, conductor creep, among others. Finally, an error propagation occurs in the prediction of temperature during a thermal transient given the uncertainty of atmospheric conditions. For instance, when the temperature in the conductor reaches the steady state after a thermal transient, it is not affected by the initial value of temperature, but only atmospheric conditions and current intensity.

III. Proposed Dynamic State Estimator

A hybrid EKF algorithm is proposed in this paper since the heat transfer phenomenon in conductors is continuous

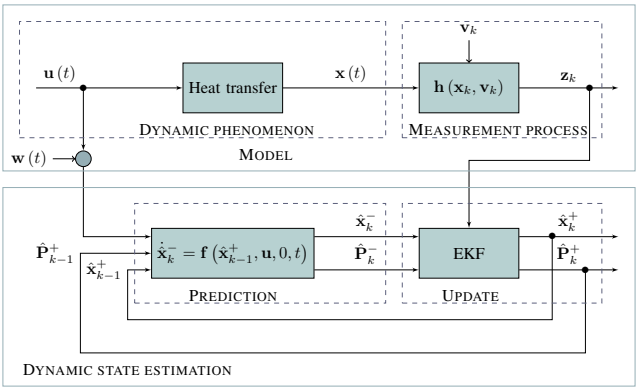

Figure 1. Proposed EKF model to estimate and predict thermal states on OHL conductors

in time, and measurements for DLR are commonly taken at discrete times. With this algorithm is aimed to estimate and predict the temperature in OHL's conductors by using both direct measurements of DLR and the atmospheric conditions. To implement an EKF is necessary to model the system $(\dot{\mathbf{x}} = \mathbf{f}(\mathbf{x}, \ldots))$, predict future states $\left(\hat{\mathbf{x}}_k^-\right)$ and update the current states $\left(\hat{\mathbf{x}}_k^+\right)$ with new measurements $(\mathbf{z}_k)$. The proposed EKF for DLR is described by means of Fig. 1 as follows:

A. System modeling

Significant errors in the prediction of the temperature during a thermal transient occur mainly because of inaccuracies in the value of wind speed under forced cooling. Additionally, the values of emissivity (ε_s) and solar absorptivity (α_s) of conductor surface can vary between 0.2 and 0.9 [21], depending on the environmental conditions and time. Hence, this paper proposes to consider $(\varepsilon_s, \alpha_s)$, along with the effective wind speed $(|\vartheta|)$ and the average conductor temperature as state variables. By assuming that OHL's thermal constant is in a time interval of 5 - 15 min and based on CIGRE recommendations [12], $|\vartheta|$ can consider as the average effective wind speed during this period and therefore assumed constant. Likewise, ε_s and α_s are assumed constant. Thus, the system can be modeled by

$$\begin{aligned} \dot{\mathbf{x}} &= \begin{bmatrix} f(\mathbf{x}, \mathbf{u}, \mathbf{w}, t) \\ 0 \\ 0 \\ 0 \end{bmatrix} \\ \mathbf{z}_k &= \mathbf{h}(\mathbf{x}_k, \mathbf{v}_k) \\ \mathbf{w}(t) &\sim (0, \mathbf{Q}) \\ \mathbf{v}_k &\sim (0, \mathbf{R}_k) \end{aligned} \tag{4}$$

where f is the function (1), $\mathbf{x}$ is the state vector, $\mathbf{u}$ is the vector of control variables, t is the time and $\mathbf{w}$ are the errors in the system. The state vector is $\mathbf{x} = \begin{bmatrix} T_S & |\vartheta| & \varepsilon_s & \alpha_s \end{bmatrix}^T$. The control variables selected are $|i_{km}|$, the ambient temperature (T_a), the wind attack angle (δ) and the solar radiation (S), i.e., $\mathbf{u} = \begin{bmatrix} |i_{km}| & T_a & \delta & S \end{bmatrix}$. Finally, the state variables are related to a set of measurements $\mathbf{z}_k$ at time k by means of measurement functions $\mathbf{h}(\mathbf{x}_k, \mathbf{v}_k)$, which have errors $\mathbf{v}_k$. The errors $\mathbf{v}_k$ and $\mathbf{w}$ are assumed to have a normal probability distribution with mean zero and covariance $\mathbf{Q}$ and $\mathbf{R}_k$.

B. Prediction of future states

To predict a future state, a system error $\mathbf{w} = 0$ is assumed and a state prediction $\left(\hat{\mathbf{x}}_k^-\right)$ is carried out at time t by

$$\begin{aligned} \dot{\hat{\mathbf{x}}}_k^- &= \begin{bmatrix} f\left(\hat{\mathbf{x}}_{k-1}^+, \mathbf{u}, 0, t\right) \\ 0 \\ 0 \\ 0 \end{bmatrix} \\ \dot{\mathbf{P}}_k^- &= \mathbf{F}\mathbf{P}_{k-1}^+ + \mathbf{P}_{k-1}^+\mathbf{F}^T + \mathbf{L}\mathbf{Q}\mathbf{L}^T \end{aligned} \tag{5}$$

taking the estimation of the current states $\left(\hat{\mathbf{x}}_{k-1}^+\right)$. $\dot{\hat{\mathbf{x}}}_k^-$ is computed by numerical integration (2). $\mathbf{P}$ is the covariance of the estimation error, $\mathbf{F}$ is the Jacobian of the model with respect to state variables $(\mathbf{F} = \partial\mathbf{f}/\partial\mathbf{x})$ calculated by

$$\mathbf{F} = \left[\begin{matrix} \frac{df}{dT_S} & \frac{df}{d\vartheta} & \frac{df}{d\varepsilon_s} & \frac{df}{d\alpha_s} \\ 0 & 0 & 0 & 0 \\ 0 & 0 & 0 & 0 \\ 0 & 0 & 0 & 0 \end{matrix} \right]\Bigg|_{\hat{\mathbf{x}},\mathbf{u}} \tag{6}$$

and $\mathbf{L}$ is the Jacobian of the model with respect to control variable errors $(\mathbf{L} = \partial\mathbf{f}/\partial\mathbf{w})$ computed using

$$\mathbf{L} = \left[\begin{matrix} \frac{df}{dw_{i_{km}}} & \frac{df}{dw_{T_a}} & \frac{df}{dw_{\delta}} & \frac{df}{dw_S} \\ 0 & 0 & 0 & 0 \\ 0 & 0 & 0 & 0 \\ 0 & 0 & 0 & 0 \end{matrix} \right]\Bigg|_{\hat{\mathbf{x}},\mathbf{u}} \tag{7}$$

C. Update of current states

The system update is performed by

$$\begin{aligned} \mathbf{K}_k &= \mathbf{P}_k^-\mathbf{H}_k^T\left(\mathbf{H}_k\mathbf{P}_k^-\mathbf{H}_k^T + \mathbf{M}_k\mathbf{R}_k\mathbf{M}_k^T\right)^{-1} \\ \hat{\mathbf{x}}_k^+ &= \hat{\mathbf{x}}_k^- + \mathbf{K}_k\left(\mathbf{z_k} - \mathbf{h}\left(\hat{\mathbf{x}}_k^-\right)\right) \\ \mathbf{P}_k^+ &= \left(\mathbf{I} - \mathbf{K}_k\mathbf{H}_k\right)\mathbf{P}_k^-\left(\mathbf{I} - \mathbf{K}_k\mathbf{H}_k\right)^T + \mathbf{K}_k\mathbf{M}_k\mathbf{R}_k\mathbf{M}_k^T\mathbf{K}_k^T \end{aligned} \tag{8}$$

using the measurements recorded at time k, where $\mathbf{K}$ is the Kalman gain, $\mathbf{H}$ is the Jacobian of the measurement functions respect to state variables $(\mathbf{H} = \partial\mathbf{h}/\partial\mathbf{x})$ calculated with

$$\mathbf{H} = \left[\frac{d\mathbf{h}}{dT_S} \quad 0 \quad 0 \quad 0 \right]\Bigg|_{\hat{\mathbf{x}}} \tag{9}$$

and $\mathbf{M}$ is the Jacobian of the measurement functions respect to measurement errors $(\mathbf{M} = \partial\mathbf{h}/\partial\mathbf{v})$ computed by

$$\mathbf{M} = \left.\frac{d\mathbf{h}(T_S)}{d\mathbf{v}}\right|_{\hat{\mathbf{x}}} \tag{10}$$

The expressions used for computing the partial derivatives of matrices $\mathbf{F}, \mathbf{L}, \mathbf{H}, \mathbf{M}$ can be found in [19]. Finally, the proposed EKF for DLR estimation is shown in algorithm 1.

Algorithm 1 Proposed algorithm for DLR Dynamic SE

procedure HYBRIDEKF($\mathbf{z}_k$,$\mathbf{u}_k$,$\hat{\mathbf{x}}^+_{k-1}$,$\mathbf{P}^+_{k-1}$,Δt,t_k,$\mathbf{Q}$,$\mathbf{R}_k$)
  $\hat{\mathbf{x}}^-_k \leftarrow \hat{\mathbf{x}}^+_{k-1}$
  $\mathbf{P}^-_k \leftarrow \mathbf{P}^+_{k-1}$
  for $j \leftarrow \Delta t$ **to** t_k **step** Δt **do** ▷ Predict
    $\dot{\hat{\mathbf{x}}}^-_k \leftarrow \mathbf{f}\left(\hat{\mathbf{x}}^-_k, u, 0, \Delta t\right)$
    $\hat{\mathbf{x}}^-_k \leftarrow \hat{\mathbf{x}}^-_k + \dot{\hat{\mathbf{x}}}^-_k$
    $\mathbf{F} \leftarrow \partial \mathbf{f}/\partial \mathbf{x}|_{\hat{\mathbf{x}}^-_k, \mathbf{u}_k}$
    $\mathbf{L} \leftarrow \partial \mathbf{f}/\partial \mathbf{w}|_{\hat{\mathbf{x}}^-_k, \mathbf{u}_k}$
    $\dot{\mathbf{P}}^-_k \leftarrow \mathbf{F}\mathbf{P}^-_k + \mathbf{P}^-_k\mathbf{F}^T + \mathbf{L}\mathbf{Q}\mathbf{L}^T$
    $\mathbf{P}^-_k \leftarrow \mathbf{P}^-_k + \dot{\mathbf{P}}^-_k$
  end for
  $\mathbf{H}_k \leftarrow \partial \mathbf{h}/\partial \mathbf{x}|_{\hat{\mathbf{x}}^-_k}$
  $\mathbf{M}_k \leftarrow \partial \mathbf{h}/\partial \mathbf{v}|_{\hat{\mathbf{x}}^-_k}$
  $\mathbf{K}_k \leftarrow \mathbf{P}^-_k\mathbf{H}^T_k\left(\mathbf{H}_k\mathbf{P}^-_k\mathbf{H}^T_k + \mathbf{M}_k\mathbf{R}_k\mathbf{M}^T_k\right)^{-1}$
  $\hat{\mathbf{x}}^+_k \leftarrow \hat{\mathbf{x}}^-_k + \mathbf{K}_k\left(\mathbf{z_k} - \mathbf{h}\left(\hat{\mathbf{x}}^-_k\right)\right)$ ▷ Update
  $\mathbf{P}^+_k \leftarrow \left(\mathbf{I} - \mathbf{K}_k\mathbf{H}_k\right)\mathbf{P}^-_k\left(\mathbf{I} - \mathbf{K}_k\mathbf{H}_k\right)^T + \mathbf{K}_k\mathbf{M}_k\mathbf{R}_k\mathbf{M}^T_k\mathbf{K}^T_k$
  return $\left(\hat{\mathbf{x}}^+_k, \mathbf{P}^+_k\right)$
end procedure

IV. Algorithm Validation

In this section, both simulations and an experimental test are performed to validate the effectiveness of the proposed EKF. Algorithm 1 was implemented in Matlab® with time steps $\Delta t = 0.1$ [s]. The EKF was evaluated in the estimation of temperature for real time monitoring and in the prediction of temperature for contingencies management as follows:

Temperature Estimation: each measurement sample was processed using the Algorithm 1, where $\hat{\mathbf{x}}^+_k$ and $\mathbf{P}^+_k$ are updated, and used as inputs for the next estimation, as shown in Fig. 1. Thus, the ability of the EKF to use the information of previous measurements is used.

Temperature Prediction: it is performed to obtain the predicted value of temperature at time $k + \Delta t_C$, where Δt_C is the assumed duration of a contingency. Thus, a temperature prediction is performed by means of (1) at time $k+\Delta t_C$ using the estimated values at time k.

A. Simulation Results

To test the algorithm with simulations, the data for temperature tracking calculation given in [21] was used, assuming a span with a length of 300 [m], having a horizontal component of conductor tension of 24.2 [kN] at 20 [°C]. To simulate the measurements and the control variables random errors $(\mathbf{v}_k, \mathbf{w})$ were added to the assumed Theor. values, as shown in Fig. 1. Normal distributions of the error with mean zero and a standard deviation (σ_{z_k}) considered as the third part of the accuracy were assumed; therefore, the variances are computed as $var\left(z_k\right) = {\sigma_{z_k}}^2$. A typical accuracy of ± 1.5 [K] [7] in the measurements of conductor temperature was used. Hence, if a maximum conductor operating temperature of 75 [°C] is used, a standard deviation of $\sigma_{T_S} = 1.5/3$ [K] in temperature measurements is equivalent to $\sigma_D = 5.5/3$ [cm] in measurements of sag and to $\sigma_H = 100/3$ [N] in measurements of mechanical tension. Finally, simulations were run with a $\Delta t_C = 15$ min and direct measurements recorded at time samples of $t_k = 1$ min.

Table I
ATMOSPHERIC CONDITIONS TAKEN FROM CIGRE GUIDE [21]

Time [min]	T_a [°C]	ϑ [m/s]	δ [°]	S [W/m^2]	$\lvert i_{km}\rvert$ [A]
$t \leq 0$	24.0	1.9	55	0	802
$0 < t \leq 10$	23.7	1.7	62	0	819
$t > 10$	23.5	0.8	37	0	856

Table II
CONDUCTORS USED FOR SIMULATIONS AND LABORATORY TEST

	Drake 26/7	Linnet	unit
Type	ACSR 26/7	ACSR 26/7	
Standard	···	ASTM B 232	
A	486.6	198.38	mm^2
d	28.1	18.31	mm
m_s	0.5119	0.217	kg/m
m_a	1.116	0.472	kg/m
$R'_{25\,°C}$	0.0727×10^{-3}	0.2095×10^{-3}	Ω/m
β_s	1×10^{-4}	1×10^{-4}	1/K
β_a	3.8×10^{-4}	3.8×10^{-4}	1/K
α_s	0.8	0.5	1
ε_s	0.8	0.5	1
α	23×10^{-6}	23×10^{-6}	1/K
$c_{s\,20\,°C}$	481	481	J/K kg
$c_{a\,20\,°C}$	897	897	J/K kg
E	57000×10^6	···	N/m^2

1) Thermal Transient System Description: a thermal transient with measurements of current intensity and atmospheric conditions provided every 10 min is assumed, as shown in Table I [21]. The conductor DRAKE ACSR (aluminum (a) and steel (s)) was used to simulate the span. Its properties are shown in Table II, where A is the cross-sectional area, d is the conductor diameter, $R'_{T_{ref}}$ is the conductor AC resistance at temperature T_{ref}, β is the linear temperature resistance coefficient and α is the coefficient of linear thermal elongation.

2) Temperature estimation and prediction: known examples were used to assess the performance of the algorithm assuming direct measurements. For simulating direct measurements, the theoretical temperature (T_S-Theor.) during transient state was computed with the values of Tables I-II by applying numerical integration (2) to the heat transfer equation (1). Equivalent values of sag and tension were computed using the values of T_S-Theor. and measurement functions [19]. Then, direct measurements were simulated with the Matlab® function *randn*, adding values of normal random errors with mean zero and equivalent standard deviation to the sag, tension and temperature. The simulated temperature measurement $z_{k=0}$ was selected to be the value of $\hat{x}^+_{k=0}$, and for the covariance the value $\hat{P}^+_{k=0} = \sigma^2$ was assumed. Since in these simulations the aim is to analyze the performance of the algorithm provided that direct measurements are available, the values of atmospheric conditions except for the wind were assumed without errors, that is $\mathbf{w}\left(t\right) = 0$. For the forecast average effective wind speed an uncertainty of ± 0.5 [m/s] was assumed ($\sigma_{|\vartheta|} = 0.5/3$ [m/s]).

To test the algorithm, two critical scenarios were modeled. The first considering a wind speed with the temperature lower limit $|\vartheta_k| = |\vartheta_k|_{\text{Theor.}} + 0.5$ [m/s] and the second one using a wind speed with the temperature upper limit $|\vartheta_k| = |\vartheta_k|_{\text{Theor.}} - 0.5$ [m/s]. Figure 2 shows the values of

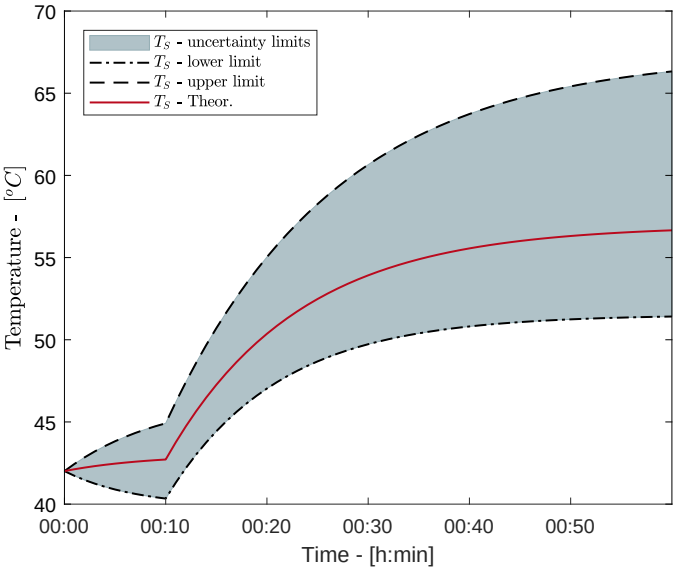

Figure 2. Both theoretical and limits of temperature of the conductor during transient state, computed with the scenarios: lower limit - $|\vartheta_k| = |\vartheta_k|_{\text{Theor.}} + 0.5$ [m/s] and upper limit - $|\vartheta_k| = |\vartheta_k|_{\text{Theor.}} - 0.5$ [m/s]

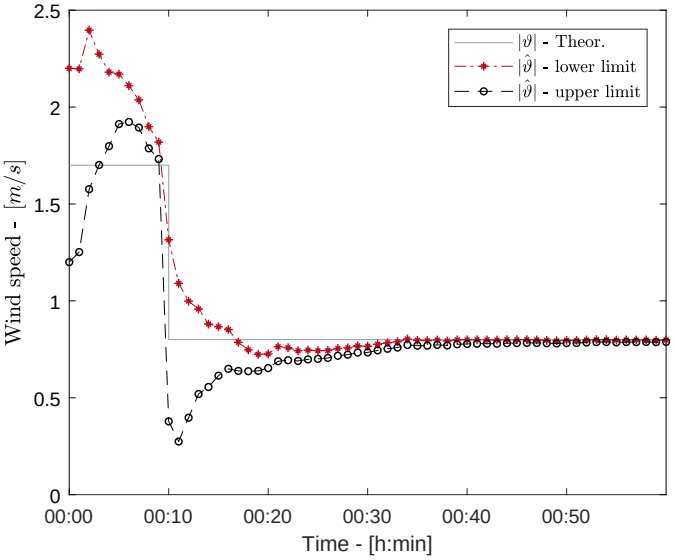

Figure 3. Theoretical wind speed $|\vartheta|$ and estimated wind speed $\left|\hat{\vartheta}\right|$ using the proposed EKF for the assumed critical scenarios

temperature during the thermal transient of T_S − Theor. and the ones for the critical scenarios. The shaded area shows the obtained uncertainty limits. To compute the root-mean-square error (RMSe), for the lower limit was 4.02 [K], and for the upper limit of 6.73 [K]. Finally, provided that the effective wind is modeled discreetly in this example, both $\left|\hat{\vartheta}_k\right| = |\vartheta_k|$ and $\hat{P}_k(2,2) = {\sigma_{|\vartheta|}}^2$ must be reset during the run of the algorithm at each time k in which the wind changes.

a) Simulations assuming temperature measurements: for simulation of direct temperature measurements, normal random errors with mean zero and $\sigma = 1.5/3$ [K] were added to the T_S-Theor. Figure 3 shows wind speed estimated for both critical cases. Figure 4 shows the values of T_S-Theor., sim-

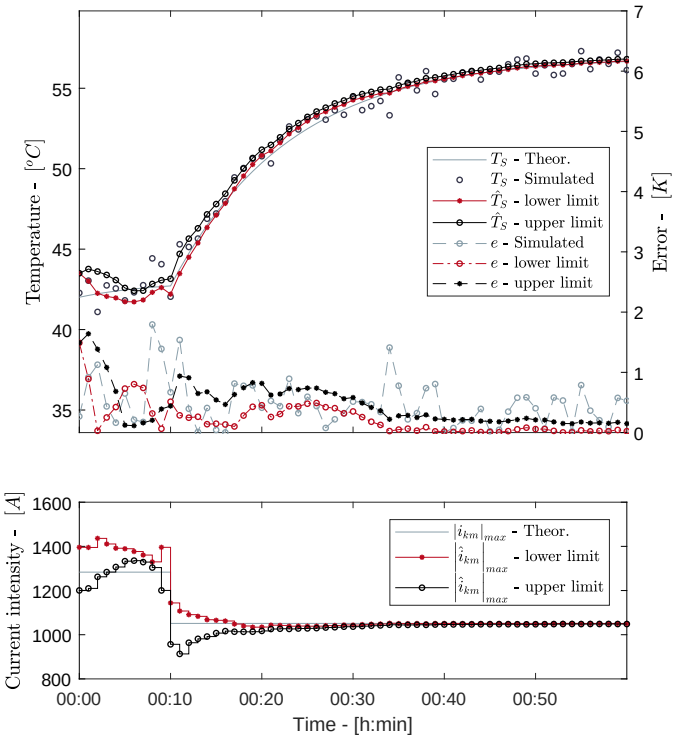

Figure 4. Temperature of the conductor (T_S-Theor.), simulations of measurements of conductor temperature (T_S Simulated), estimated temperatures $\left(\widehat{T}_S\right)$ and maximum allowable current intensity $\left(|i_{km}|_{max}\right)$ at steady state using the proposed algorithm during the thermal transient

ulations of measured temperature and estimated temperature using the proposed algorithm with the two critical cases. The error e is computed with respect to the T_S-Theor. The RMSe for the estimated temperature was 0.34 [K] taking the lower limit, and 0.54 [K] taking the upper limit. The RMSe using simulations of direct temperature measurements was 0.6 [K]. Additionally, Fig. 4 shows the maximum allowable current intensity at steady state for a temperature of 75 [°C]. The current intensity was computed with (3) using the conditions of instant k for each scenario. Figure 5 shows predicted values both of temperature and of maximum current allowable during a contingency, obtained a RMSe for the lower limit of 1.6 [K], and 2.2 [K] for the upper limit.

b) Simulations assuming tension measurements: for simulating tension measurements, errors were added as done in the previous simulation using an accuracy of 100 [N]. Figure 6 shows the simulations of measured tension (H), T_S-Theor., and the estimated temperature with the proposed algorithm. The RMSe of both estimated and predicted temperature for the lower limit were 0.18 [K] and 1.5 [K], and for the upper limit were 0.22 [K] and 2 [K] respectively.

c) Simulations assuming sag measurements: as in the case of tension measurements, Fig. 7 shows the performance of the algorithm when sag measurements are available. The RMSe of both estimated and predicted temperature for the lower and the upper limits were 0.28 [K] and 1.5 [K], and 0.29 [K] and 1.5 [K] respectively.

Finally, 1000 simulations for each one of the three direct measurements were performed. To simulate a more realistic

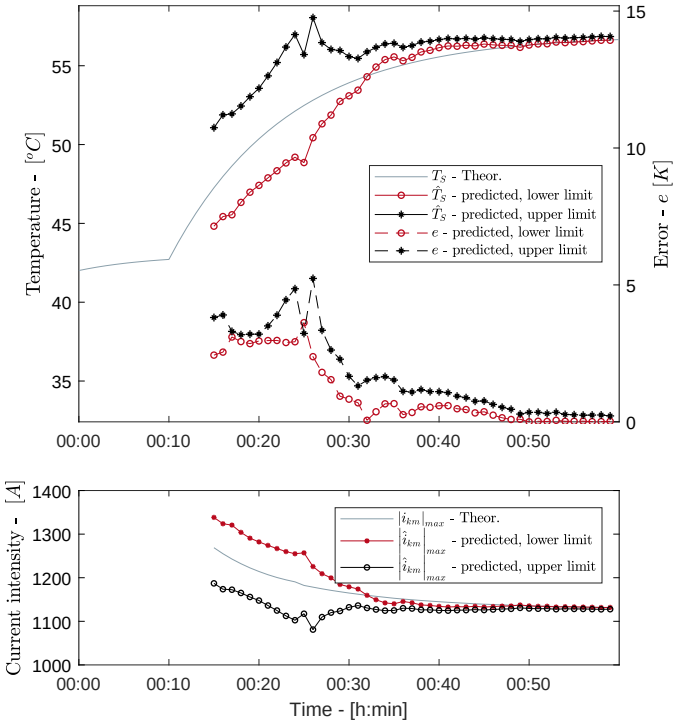

Figure 5. Temperature of the conductor (T_S-Theor.), and predictions 15 min before of temperature and maximum allowable current intensity during a contingency computed with the proposed algorithm, simulating measurements of conductor temperature

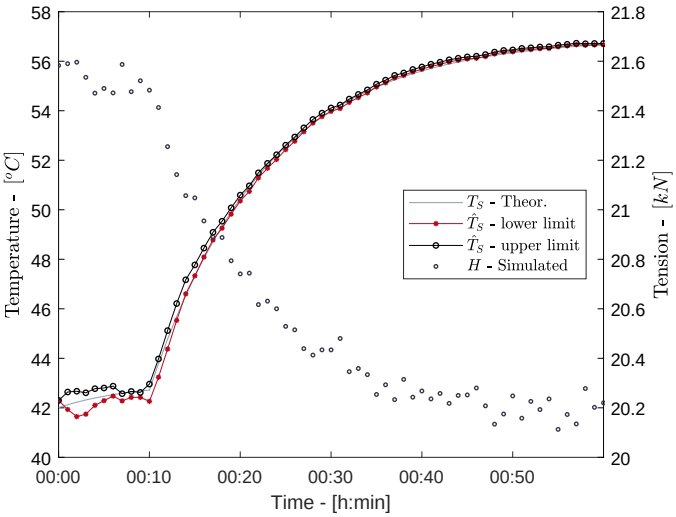

Figure 6. Simulation of mechanical tension (H), and estimated temperature $\left(\widehat{T}_S\right)$ using the proposed algorithm simulating measurements of tension on the conductor

case, errors were added on control variables, since these are commonly measured or assumed. Thus, normal random errors with mean zero were added to current intensity ($|i_{km}|$) with $\sigma = 5/3$ [A], to ambient temperature (T_a) with $\sigma = 1/3$ [K], and to wind attack angle (δ) with $\sigma = 12.5/3$ [°]. These standard deviations were taken from [19]. Table III shows the average RMSe and the average computing time to run Algorithm 1. As result, the proposed algorithm showed stability, convergence and speed, and it reached a smaller error in

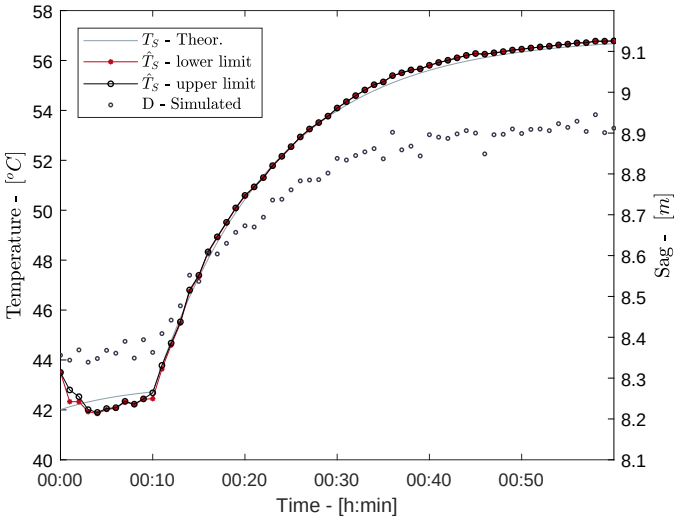

Figure 7. Simulation of sag length (D), and estimated temperature $\left(\widehat{T}_S\right)$ using the proposed algorithm simulating measurements of sag on the catenary

Table III
COMPARISON PERFORMANCE BETWEEN THE THREE KINDS OF DIRECT MEASUREMENTS FOR 1000 RANDOM CASES

Measurement	Avg. RMSe [K]	Avg. Time [s]
Temperature	0.303	0.0593
Tension	0.253	0.0598
Sag	0.328	0.0602

temperature values than in the case of using only records of direct measurements.

Although the standard deviation for δ was taken using typical anemometers accuracy, this value is unrealistic, because of wind turbulence along the stringing section. However, to estimate the average effective wind speed instead of spot values, the effect of wind turbulence is considered [12].

B. Experimental Results

A laboratory setup was designed to evaluate the algorithm. The setup consisted of controllably injecting a current intensity through the OHL conductor Linnet and measuring its temperature. The properties of the conductor are shown in Table II. To carry out the validation, an ambient temperature of $T_a = 19$ [°C], and the planned current intensity ($|i_{km}|$) and the wind ($|\vartheta|$) shown in Fig. 8 were assumed as forecast values throughout the test. An auto-transformer and a fan were used to control both $|i_{km}|$ and $|\vartheta|$. As in the simulations, the two critical cases in the estimation and prediction of the temperature were used. Additionally, a value of emissivity $\epsilon_s = 0.9$ was used as initial parameter for the lower limit and a value of emissivity $\epsilon_s = 0.2$ for the upper limit. Thus, three different cases were analyzed: **case 1** using the assumed planned and forecasted values, **case 2** using the upper limits, and **case 3** using the lower limits.

1) Test setup: considering the laboratory atmospheric conditions, the conductor under test theoretically reaches 75 [°C] with an $|i_{km}|$ of almost 500 [A]. Taking the limitations of the short circuit current of the laboratory into account, a special

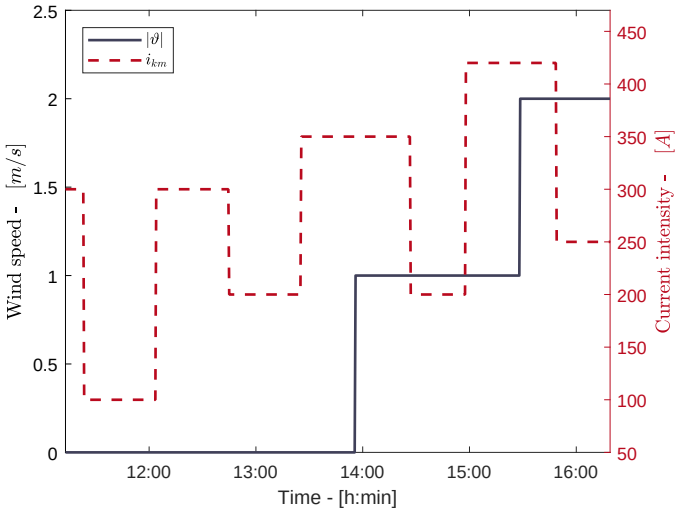

Figure 8. Current intensity planned ($|i_{km}|$) and forecasted wind speed ($|\vartheta|$) used in the test

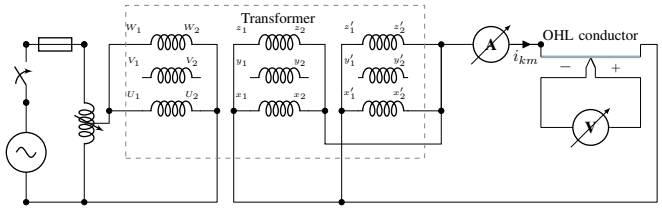

Figure 9. Circuit diagram of the experimental test

three-winding three-phase distribution transformer (HV-LV-LV) with open ends was used to reach this current, as shown in Fig. 9. The setup used is shown in Fig. 10. To reduce the influence of loop impedance the leads were located almost perpendicular to the conductor and the transformer was about 1 [m] away.

2) Test Results: the setup was initially energized with 300 [A], and when the conductor reached the thermal steady state, the planned conditions (Fig. 8) were controlled and the variables $|i_{km}|$, T_S and T_a were measured and recorded every 30 [s] with an accuracy of ± 5 [A] and ± 1.5 [K]. Measurements are shown in Fig. 11. Since the test was carried out indoors, the solar radiation was assumed to be $S = 0$.

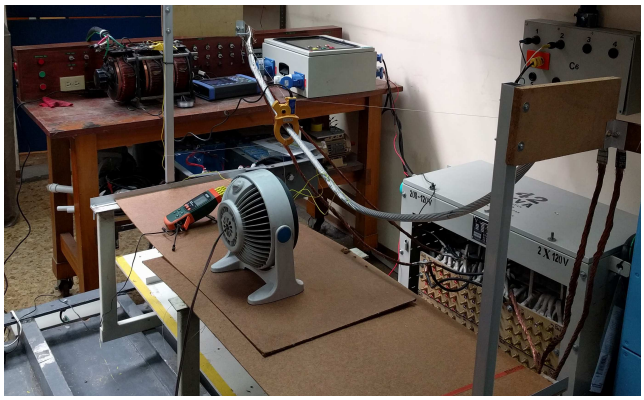

Figure 10. Experimental test setup

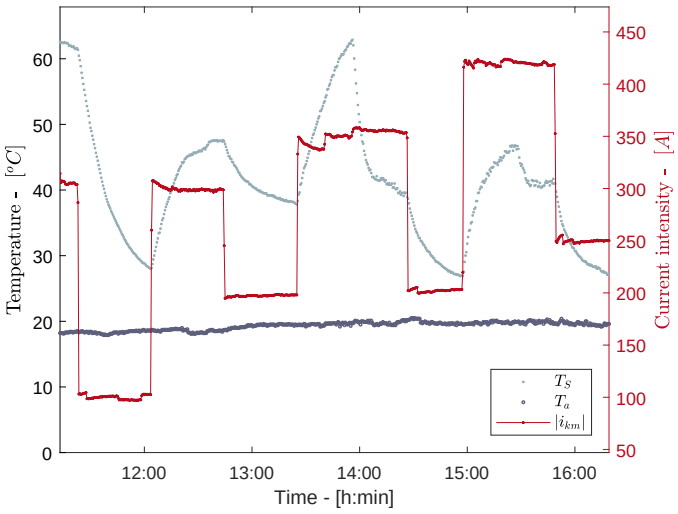

Figure 11. Measurements of current intensity ($|i_{km}|$), temperature of the conductor (T_S) and ambient temperature (T_a) recorded every 30 [s]

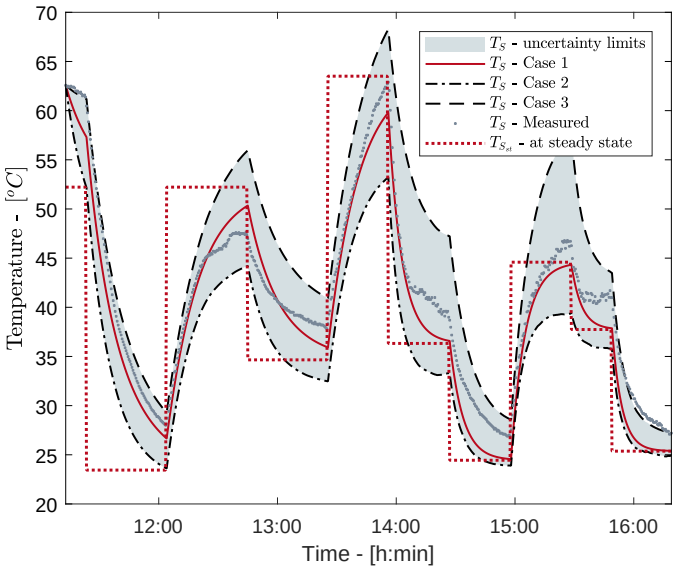

Figure 12. Comparison of temperature measured and computed with planned and forecasted conditions, upper limit and lower limit

Figure 12 shows the values of temperature computed using (2) for the three cases and the temperature measured. The Root mean square residuals (RMSϵ) obtained were RMS$\epsilon = 2.4$ [K] for case 1, RMS$\epsilon = 5.7$ [K] case 2 and RMS$\epsilon = 5.5$ [K] for case 3.

3) Estimation of average Temperature: The values estimated both of effective wind speed and emissivity of the conductor using the proposed EKF in each case are shown in Fig. 13. The estimated average conductor temperature for the case with the highest RMSϵ (case 2) is shown in Fig. 14. A RMS$\epsilon = 1.5$ [K] was obtained with this estimated temperature.

4) Prediction of Temperature: Taking the case 2, the temperature predicted 15 min before is shown in Fig. 15. In this temperature prediction, a $RMS\epsilon = 2.5$ [K] was obtained. Additionally, Fig. 15 shows the maximum current intensity

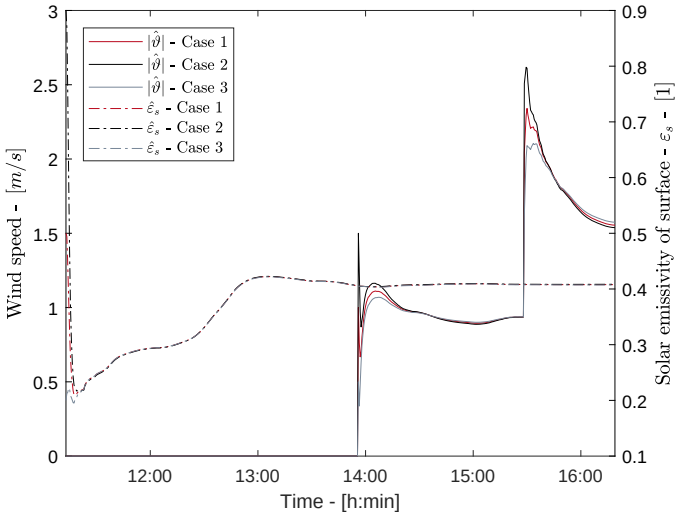

Figure 13. Estimated effective wind speed $\left(\left|\hat{\vartheta}\right|\right)$ and emissivity $(\hat{\epsilon}_s)$ for each case

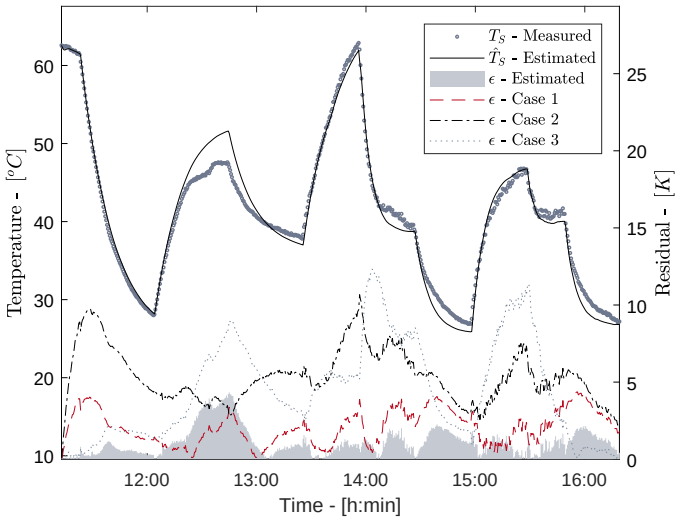

Figure 14. Comparison of estimated averaged temperature and measured temperature, and comparison of residual of estimated and computed temperature in each case

allowable until the conductor reaches 75 [°C]. This current intensity was predicted 15 min before.

V. Conclusions

This paper presents an algorithm to estimate and predict thermal transient states in OHL conductors and addresses its implementation. This algorithm uses an EKF based on the heat transfer equation, using atmospheric conditions, current intensity, conductor parameters and direct measurements as inputs. The uncertainty in these values was considered. To simulate and test the EKF, the algorithm estimated and predicted values of average conductor temperature, with processing times lower than the time spent between measurement samples, showing computational efficiency and stability. The algorithm can be directly implemented on current DLR systems in a fast and cost-effective way.

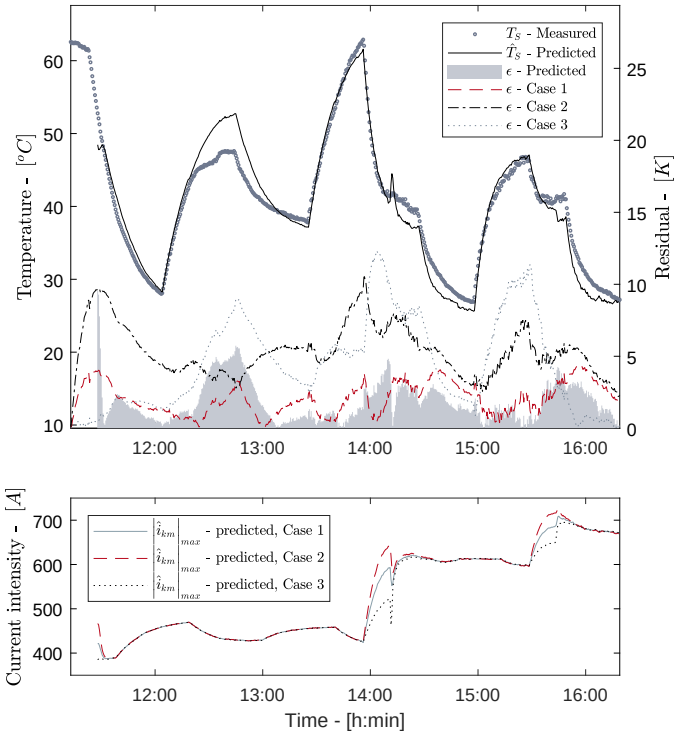

Figure 15. Comparison between the average temperature predicted 15 min before and temperature measured, comparison between residual of predicted average temperature and temperature computed in each case, and maximum current intensity allowable until the conductor reaches 75 [°C]

Average effective wind speed, emissivity and solar absorptivity were chosen as parameters to be estimated, due to the impact of their uncertainty on heat transfer. Effective wind speed was assumed constant during a typical time of contingency. Nevertheless, models of wind behavior for long time emergency could be included in future studies.

The algorithm assessment showed a reduction in the RMEe and RMSϵ when thermal estimation and prediction are carried out by the proposed EKF, allowing to increase the reliability in the thermal monitoring of OHLs. For instance, despite using the most critical case, the RMSe obtained using the algorithm to estimate and predict the average conductor temperature was less than the RMSe obtained in all cases, both the simulations and the experiment. The algorithm validation was performed using low wind speeds which is considered a critical scenario. In the cases of higher wind speeds and low current intensities where the conductor temperature is close to the ambient temperature, a field test validation is necessary. Finally, further analysis should be carried out using data validation techniques.

Acknowledgment

This research was supported by the Colombian Department of Science, Technology and Innovation (Colciencias) under the project 617 - National Doctorates.

References

[1] CIGRE WG B2.13, "Guidelines for increased Utilization of existing Overhead Transmission Lines," Technical Brochure 353. Paris: CIGRE, 2008.

[2] D. Douglass, W. Chisholm, G. Davidson, I. Grant, K. Lindsey, M. Lancaster, D. Lawry, T. McCarthy, C. Nascimento, M. Pasha, J. Reding, T. Seppa, J. Toth, and P. Waltz, "Real-Time Overhead Transmission-Line Monitoring for Dynamic Rating," *IEEE Transactions on Power Delivery*, vol. 31, no. 3, pp. 921–927, jun 2016. [Online]. Available: http://ieeexplore.ieee.org/document/6991585/

[3] D. Koval and R. Billinton, "Determination of Transmission Line Ampacities by Probability and Numerical Methods," *IEEE Transactions on Power Apparatus and Systems*, vol. PAS-89, no. 7, pp. 1485–1492, sep 1970. [Online]. Available: http://ieeexplore.ieee.org/document/4074224/

[4] I. Cotton and J. Teh, "Critical span identification model for dynamic thermal rating system placement," *IET Generation, Transmission & Distribution*, vol. 9, no. 16, pp. 2644–2652, dec 2015. [Online]. Available: http://digital-library.theiet.org/content/journals/10.1049/iet-gtd.2015.0601

[5] M. Matus, D. Saez, M. Favley, C. Suazo-Martinez, J. Moya, G. Jimenez-Estevez, R. Palma-Behnke, G. Olguin, and P. Jorquera, "Identification of Critical Spans for Monitoring Systems in Dynamic Thermal Rating," *IEEE Transactions on Power Delivery*, vol. 27, no. 2, pp. 1002–1009, apr 2012. [Online]. Available: http://ieeexplore.ieee.org/document/6163401/

[6] J. L. Aznarte and N. Siebert, "Dynamic Line Rating Using Numerical Weather Predictions and Machine Learning: A Case Study," *IEEE Transactions on Power Delivery*, vol. 32, no. 1, pp. 335–343, feb 2017. [Online]. Available: http://ieeexplore.ieee.org/document/7442844/

[7] CIGRE WG B2.36, "Guide for Application of Direct Real-Time Monitoring Systems," Technical Brochure 498. Paris: CIGRE, 2012.

[8] A. Michiorri, H.-M. Nguyen, S. Alessandrini, J. B. Bremnes, S. Dierer, E. Ferrero, B.-E. Nygaard, P. Pinson, N. Thomaidis, and S. Uski, "Forecasting for dynamic line rating," *Renewable and Sustainable Energy Reviews*, vol. 52, pp. 1713–1730, dec 2015. [Online]. Available: http://linkinghub.elsevier.com/retrieve/pii/S1364032115007819

[9] I. Albizu, E. Fernandez, P. Eguia, E. Torres, and A. J. Mazon, "Tension and Ampacity Monitoring System for Overhead Lines," *IEEE Transactions on Power Delivery*, vol. 28, no. 1, pp. 3–10, jan 2013. [Online]. Available: http://ieeexplore.ieee.org/document/6313952/

[10] C. R. Black and W. A. Chisholm, "Key Considerations for the Selection of Dynamic Thermal Line Rating Systems," *IEEE Transactions on Power Delivery*, vol. 30, no. 5, pp. 2154–2162, oct 2015. [Online]. Available: http://ieeexplore.ieee.org/document/6967802/

[11] I. Albizu, E. Fernandez, A. Mazon, and J. Bengoechea, "Influence of the conductor temperature error on the overhead line ampacity monitoring systems," *IET Generation, Transmission & Distribution*, vol. 5, no. 4, p. 440, 2011. [Online]. Available: http://digital-library.theiet.org/content/journals/10.1049/iet-gtd.2010.0470

[12] CIGRE WG B2.12, "Guide for Selection of Weather Parameters for Bare Overhead Conductor Ratings," Technical Brochure 299. Paris: CIGRE, 2006.

[13] A. Piccolo, A. Vaccaro, and D. Villacci, "Thermal rating assessment of overhead lines by Affine Arithmetic," *Electric Power Systems Research*, vol. 71, no. 3, pp. 275–283, nov 2004. [Online]. Available: http://linkinghub.elsevier.com/retrieve/pii/S0378779604000677

[14] M. A. Bucher and G. Andersson, "Robust Corrective Control Measures in Power Systems With Dynamic Line Rating," *IEEE Transactions on Power Systems*, vol. 31, no. 3, pp. 2034–2043, may 2016. [Online]. Available: http://ieeexplore.ieee.org/document/7163367/

[15] A. Polevoy, "Impact of Data Errors on Sag Calculation Accuracy for Overhead Transmission Line," *IEEE Transactions on Power Delivery*, vol. 29, no. 5, pp. 2040–2045, oct 2014. [Online]. Available: http://ieeexplore.ieee.org/document/6828800/

[16] E. Carlini, G. Giannuzzi, C. Pisani, A. Vaccaro, and D. Villacci, "Experimental deployment of a self-organizing sensors network for dynamic thermal rating assessment of overhead lines," *Electric Power Systems Research*, vol. 157, pp. 59–69, apr 2018. [Online]. Available: http://linkinghub.elsevier.com/retrieve/pii/S0378779617304789

[17] A. Michiorri, P. C. Taylor, and S. C. E. Jupe, "Overhead line real-time rating estimation algorithm: Description and validation," *Proceedings of the Institution of Mechanical Engineers, Part A: Journal of Power and Energy*, vol. 224, no. 3, pp. 293–304, may 2010. [Online]. Available: http://journals.sagepub.com/doi/10.1243/09576509JPE859

[18] E. Carlini, C. Pisani, A. Vaccaro, and D. Villacci, "A reliable computing framework for dynamic line rating of overhead lines," *Electric Power Systems Research*, vol. 132, pp. 1–8, mar 2016. [Online]. Available: http://linkinghub.elsevier.com/retrieve/pii/S0378779615003302

[19] D. L. Alvarez, F. Faria da Silva, E. E. Mombello, C. L. Bak, J. A. Rosero, and D. L. Ólason, "An approach to dynamic line rating state estimation at thermal steady state using direct and indirect measurements," *Electric Power Systems Research*, dec 2017. [Online]. Available: http://linkinghub.elsevier.com/retrieve/pii/S0378779617304595

[20] D. Simon, "Nonlinear Kalman filtering," in *Optimal State Estimation Kalman, H Infinity, and Nonlinear Approaches*. Hoboken, NJ, USA: John Wiley & Sons, Inc., may 2006, ch. 13, pp. 395–426. [Online]. Available: http://doi.wiley.com/10.1002/0470045345

[21] CIGRE WG B2.42, "Guide for thermal rating calculations of overhead lines," Technical Brochure 601. Paris: CIGRE, 2014.

[22] V. T. Morgan, *Thermal Behaviour of Electrical Conductors: Steady, Dynamic, and Fault-current Ratings*. Research Studies Press, 1991.

[23] IEEE Std 738-2006, *IEEE Standard for Calculating the Current-Temperature of Bare Overhead Conductors*, 2007.